

tope effect is consistent with accepted classical and quantum mechanical models. This Letter also provides a scaling relationship accurate at intermediate energies for differential electron-capture cross sections which is expected to be applicable to other types of differential cross sections involving hydrogen-isotope projectiles.

This work was supported in part by the National Science Foundation and by the U. S. Department of Energy—Office of Magnetic Fusion Energy. The authors wish to thank L. Newquist, D. Seely, and T. Streeter for their assistance in obtaining the experimental data.

¹H. B. Gilbody, in *Advances in Atomic and Molecular Physics*, edited by D. R. Bates and B. Bederson (Academic, New York, 1975), Vol. 15, p. 293.

²F. J. de Heer, in *Atomic and Molecular Processes in Controlled Thermonuclear Fusion*, edited by M. R. C. McDowell and A. M. Ferendeci (Plenum, New York, 1979), p. 351.

³J. H. Newman, J. D. Cogan, D. L. Ziegler, D. E. Nitz, R. D. Rundel, K. A. Smith, and R. F. Stebbings, *Phys. Rev. A* **25**, 2976 (1982).

⁴D. R. Bates, H. S. W. Massey, and A. L. Stewart, *Proc. Roy. Soc. London, Ser. A* **216**, 437 (1953).

⁵P. J. Martin, K. Arnett, D. M. Blankenship, T. J. Kvale, J. L. Peacher, E. Redd, V. C. Sutcliffe, J. T. Park, C. D. Lin, and J. H. McGuire, *Phys. Rev. A* **23**, 2858 (1981).

⁶J. T. Park, J. E. Aldag, J. L. Peacher, and J. M. George, *Phys. Rev. A* **21**, 751 (1980).

⁷P. J. Martin, D. M. Blankenship, T. J. Kvale, E. Redd, J. L. Peacher, and J. T. Park, *Phys. Rev. A* **23**, 3357 (1981).

⁸W. L. Fite, R. T. Brackmann, and W. R. Snow, *Phys. Rev.* **112**, 1161 (1958).

⁹J. T. Park, J. M. George, J. L. Peacher, and J. E. Aldag, *Phys. Rev. A* **18**, 48 (1978).

¹⁰R. E. Olson and A. Salop, *Phys. Rev. A* **16**, 531 (1977).

¹¹R. Abrines and I. C. Percival, *Proc. Phys. Soc.* **88**, 861 (1966).

¹²G. W. McClure, *Phys. Rev.* **148**, 47 (1966).

¹³M. R. C. McDowell and J. P. Coleman, *Introduction to the Theory of Ion-Atom Collisions* (North-Holland, Amsterdam, 1970), Chaps. 6 and 8.

Resistive-Wall Destabilization of Diocotron Waves

W. D. White, J. H. Malmberg, and C. F. Driscoll

Department of Physics, University of California, San Diego, La Jolla, California 92093

(Received 3 September 1982)

The growth of the negative-energy $l = 1$ diocotron wave has been studied on a column of pure electron plasma. An external RC circuit connecting sectors of the bounding wall is used to induce growth of the wave, which is otherwise essentially neutrally stable. Such a circuit also causes small shifts in the real part of the wave frequency. The experimentally measured growth rates and frequency shifts are in close agreement with the predictions of theory over a wide range of experimental parameters.

PACS numbers: 52.35.Py, 52.35.Fp

The stability properties of diocotron waves affect the operation of many magnetized charged-particle systems, such as electron beams,^{1,2} magnetrons,^{3,4} and Penning discharges.⁵ The diocotron waves are $\vec{E} \times \vec{B}$ drift waves propagating in a nonneutral plasma. Some of these waves lower the electrostatic potential energy of the system and may grow if energy is dissipated by the image currents induced in boundary walls. The release of potential energy by this mechanism is analogous and complementary to the release of kinetic energy seen in the resistive-wall

instability of negative-energy plasma waves in a beam.⁶ In our case, growth rates can be predicted on the basis of energy conservation.⁷ Further, a calculation considering a complex wall impedance as a boundary-value perturbation on the wave predicts a complex wave-frequency shift proportional to the impedance.

Here, we report experimental data on the resistive-wall destabilization of diocotron waves with azimuthal mode number $l = 1$. The waves are observed on a confined, quiescent pure-electron-plasma column.⁸⁻¹⁰ In this system, the $l = 1$

diocotron waves normally show negligible damping during the course of our measurements, while waves with $l \geq 2$ are strongly damped.^{7,9} An external impedance connected between two sectors of the bounding wall is used to induce growth of the $l=1$ wave. Agreement with theory to within 10% is typically found for the measured growth rates and real-part frequency shifts of the wave.

The containment apparatus is shown schematically in Fig. 1. The entire apparatus is in a uniform axial magnetic field B , and evacuated to 5×10^{-10} Torr. The electrostatic boundary is a piecewise conducting wall at radius $R_w = 3.05$ cm; the wall consists of a series of twelve electrically isolated cylinders of various lengths (for the sake of clarity, only three are shown in Fig. 1). A few of these wall cylinders are divided into angular sectors which are used to launch or detect waves having azimuthal ($e^{i\theta}$) dependence; the sectors are also used to provide resistive loading on the diocotron wave.

Electrons emitted from a dc-heated spiral tungsten filament are trapped by sequential application of negative voltages to two of the cylinders, e.g., 3 and then 1. This results in an axisymmetric electron plasma column several Debye lengths in radius, with a bell-shaped radial density profile having central density $\approx 1.4 \times 10^7$ cm⁻³, radius $R_p \approx 1.4$ cm, and average thermal energy ≈ 1 eV.⁸⁻¹⁰ The electron plasma contains a negligible number of ions, since ions are not confined longitudinally. The bell-shaped density profile is responsible for rapid damping of waves with $l \geq 2$,^{7,9} and the absence of the hollow-beam diocotron instability.⁴ The radial electric field due to the space charge gives the plasma an $\vec{E} \times \vec{B}$ drift rotation in the $\hat{\theta}$ direction. The ratio of the rotation frequency ω_E to the plasma frequency is small ($\omega_E / \omega_p \sim \omega_p / 2\Omega_c \approx 0.1$). The length of the plasma column can be varied over the range $12 \leq L \leq 120$

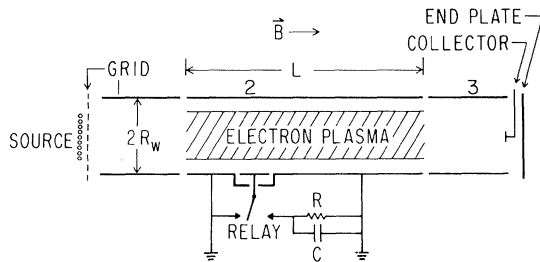


FIG. 1. The cylindrical confinement apparatus, with a switched impedance on one sector of the wall.

cm by use of the different cylinders for containment.

After the plasma is trapped, the relay shown in Fig. 1 is switched to connect an external impedance between a sector and the rest of the wall. This induces wave growth as shown in Fig. 2. A small-amplitude $l=1$ diocotron wave (partially hidden in receiver noise) is initially present, as a result of asymmetries in the injection process.⁹ When the relay introduces a nonzero wall impedance, the wave power grows exponentially with time, as $\exp(2\delta\omega_i t)$. When the sector is again shorted to the rest of the wall, the large-amplitude wave shows only weak damping, which may be related to the slow evolution of the plasma column.⁹

At the end of an observation cycle, the plasma is dumped out axially. A movable collector and many repetitions of this cycle are used to determine the density profile. If density measurement is timed to be synchronous with wave phase, a displacement of the profile with negligible spreading is observed. In real time, this displacement rotates at the wave frequency and grows as the wave grows. The wave grows in the simple manner described until the tail of the density distribution scrapes the wall, resulting in electron loss, decrease of wave frequency, rapid wave damping, and spreading of the profile.

The wave evolution described above was measured by sampling the wave power at varying times in many similar plasma samples, so that the additional 50- Ω impedance of the receiver is connected to a sector for only a short observation time each cycle. The 0.5-dB jitter at high power shows the degree of cycle-to-cycle reproducibility of the plasma samples.

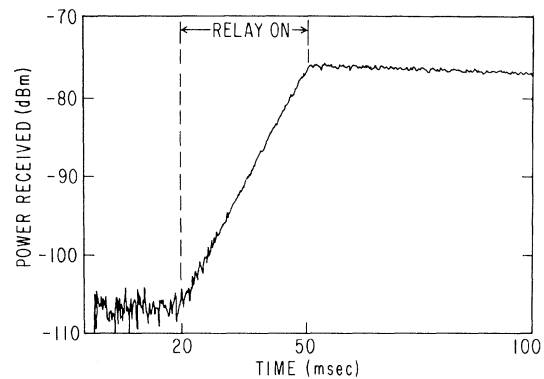


FIG. 2. Received power vs time for a resistively destabilized $l=1$ diocotron mode.

The growth rate expected for this destabilized diocotron wave can be obtained from a simple model comparing the negative energy of the wave to the power dissipated in the resistor.⁷ The model treats the plasma as a cold fluid in $\vec{E} \times \vec{B}$ motion. The neglect of temperature effects is justified since the gyroradius is small compared with the column radius and the axial wavelength is long. For the case of an infinitely long plasma column and a perfectly conducting wall at $r = R_w$, the $l = 1$ diocotron potential is¹¹

$$\delta\varphi(r, \theta, t) = S \frac{r}{2} \left(\frac{\omega_E(r) - \omega}{\omega} \right) \cos(\theta - \omega t). \quad (1)$$

The wave frequency ω is real and equal to the $\vec{E} \times \vec{B}$ rotation rate at the radius of the wall:

$$\omega = \omega_E(R_w), \quad (2)$$

where

$$\omega_E(r) = (e/\epsilon_0 B r^2) \int_0^r r' dr' n(r'). \quad (3)$$

The amplitude of the wave has been normalized such that the radial electric field at the wall is $S \cos(\theta - \omega t)$.

This wave is exceptionally simple. Unlike higher- l diocotron waves, this wave has no resonant particles since the resonant radius is at the wall. Moreover, the wave frequency depends only on total charge and not the density profile. Finally the density

$$\delta n(r, \theta, t) \propto \nabla^2 \delta\varphi \propto \frac{dn^0(r)}{dr} \cos(\theta - \omega t)$$

is recognizable as the linear term for the observed displacement of the column.

The decrease in electrostatic energy due to such a displacement of the charge is $-\pi\epsilon_0 R_w^2 S^2/4$ joule per meter of column length, which may be calculated either from a dielectric tensor formalism,⁷ or directly from the charge displacement in its self-consistent electric field. We neglect "end effects" and write the wave energy in a trapped electron column of length L as

$$\delta W = -L(\pi\epsilon_0 R_w^2 S^2/4). \quad (4)$$

For comparison between measurements and the theory, we will take the value of L to be the length of the containment cylinder.

Now if the wall sector is connected to the external RC circuit as shown in Fig. 1, the wave will drive current in the circuit by inducing surface charge on the sector probe. The power dis-

sipated in the resistor is

$$P = \frac{1}{2} I^2 \text{Re} Z \\ = \frac{1}{2} [2\epsilon_0 \omega S L_s R_w \sin(\frac{1}{2}\Delta\theta)]^2 \left(\frac{R}{1 + \omega^2 R^2 C^2} \right), \quad (5)$$

where I is the amplitude of the induced sinusoidal current, Z is the complex circuit impedance, and L_s and $\Delta\theta$ are the length and angular size of the sector. The wave amplitude will grow as $\exp(\delta\omega_i \times t)$, where the growth rate is given by energy conservation as

$$\delta\omega_i = -\frac{P}{2\delta W} \\ = \frac{4\epsilon_0}{\pi} \frac{\omega^2 L_s^2 \sin^2(\frac{1}{2}\Delta\theta)}{L} \left(\frac{R}{1 + \omega^2 R^2 C^2} \right). \quad (6)$$

Correspondingly, the imaginary part of the wall impedance leads to a shift in the real part of the wave frequency. To calculate this frequency shift, we have done a standard first-order perturbation theory, with the effect of wall impedance included as a boundary condition. This theory generalizes Eq. (6) to predict a complex frequency $\delta\omega$ given by

$$\delta\omega = \delta\omega_r + i\delta\omega_i \\ = \frac{i4\epsilon_0}{\pi} \frac{\omega^2 L_s^2 \sin^2(\frac{1}{2}\Delta\theta)}{L} \left[\frac{R + i\omega R^2 C}{1 + \omega^2 R^2 C^2} \right], \quad (7)$$

under the assumption $|\delta\omega/\omega| \ll 1$. Note that the term in square brackets is just the complex impedance of the external circuit. The wave growth and frequency shift depend only on the wave frequency, on geometric factors, and on the real and imaginary parts of the external impedance.

The predictions of Eq. (7) have been verified experimentally in all essential respects. Figure 3 shows the measured growth rate of the wave as a function of the external resistance R , for

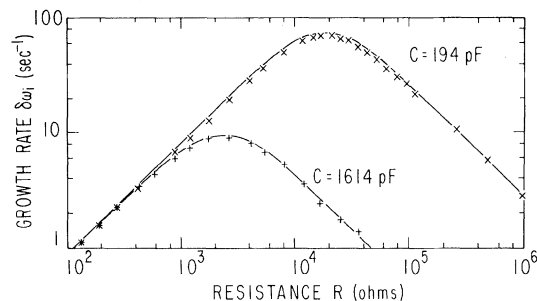


FIG. 3. Measured wave growth rate vs the resistance of the wall circuit, for two values of the circuit capacitance. The lines are the predictions of Eq. (7).

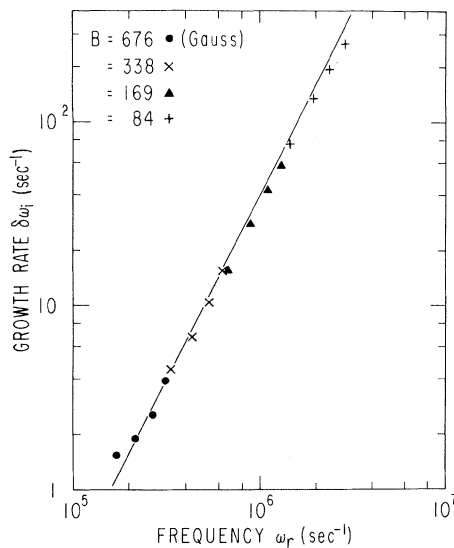


FIG. 4. Wave growth rate vs measured wave frequency, keeping the real part of the load impedance constant.

two values of the capacitance C . The solid curves in the figure are the absolute predictions of Eq. (7) based on the measured values of ω , L_s , $\Delta\theta$, and the length L of the containment cylinder. The growth rate is proportional to the real part of the external impedance.

Figure 4 shows the measured growth rate $\delta\omega_i$ as a function of the measured wave frequency ω_r . The different wave frequencies were obtained by varying the magnetic field, and also by varying the bias voltage of the source, thereby changing the plasma radial density profile. As the frequency was changed, the resistor was adjusted as necessary to keep the real part of the load impedance constant. The solid line is again the absolute prediction of Eq. (7). Finally, the dependence of the growth rate on $\Delta\theta$, L , and L_s has also been checked, by using sectors of angular size $\Delta\theta = 30, 60, 90, 120, 150,$ and 180 deg, seven different containment lengths with $12 \leq L \leq 120$ cm, and $L_s = 3.05$ and 6.1 cm. Agreement with theory is within 10%.

The impedance of the external circuit can be made essentially capacitive by choosing a large value of R , so that $\omega RC \gg 1$. Equation (7) then predicts a downward shift in the real wave frequency, with $\delta\omega_r/\omega_r \propto C^{-1}$. To measure this frequency shift, we count the received wave cycles during set intervals with and without the external impedance connected. For each plasma sample, the counts from two such intervals are subtracted

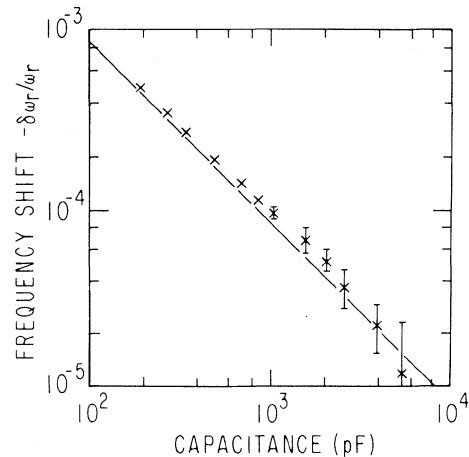


FIG. 5. Wave-frequency shift vs the capacitance of the wall circuit.

to obtain a frequency difference. The order of the intervals is reversed with each new plasma sample, and the frequency differences are averaged over 10^3 plasma samples to obtain $\delta\omega_r$.

Figure 5 shows the measured frequency shift $\delta\omega_r/\omega_r$ as a function of the circuit capacitance C . The error bars represent 1 standard deviation from five groups of 1000 plasma samples each. The solid line is the absolute prediction of Eq. (7). The agreement is within the accuracy of the experiments.

In summary, we have shown that a resistive-wall impedance can drive the negative-energy $l = 1$ diocotron wave unstable in an otherwise quiescent, confined electron plasma. The growth-rate data agree within 10% with theory over the entire range of experimental parameter variations. We regard this agreement as satisfactory since the accuracy of these experimental measurements is approximately 10%, and since there may also be effects of this magnitude left out of the simple theoretical model. When the wall impedance is capacitive, we measure a real frequency shift for the wave, again in agreement with theory.

We wish to acknowledge many enlightening discussions with J. S. deGrassie and S. A. Prasad. This work is based on research supported by the National Science Foundation under Grant No. PHY 80-09326.

¹R. C. Davidson, *Theory of Nonneutral Plasmas* (Benjamin, Reading, Mass., 1974).

²C. A. Kapetanacos, D. A. Hammer, C. D. Striffler, and R. C. Davidson, *Phys. Rev. Lett.* **26**, 1303 (1973).

³O. Buneman, R. H. Levy, and L. M. Linson, *J. Appl. Phys.* **37**, 3203 (1966).

⁴R. H. Levy, *Phys. Fluids* **8**, 1268 (1965).

⁵W. Knauer, *J. Appl. Phys.* **37**, 602 (1966).

⁶C. K. Birdsall and J. R. Whimery, *J. Appl. Phys.* **24**, 314 (1953); C. K. Birdsall, G. R. Brewer, and A. V. Haeff, *Proc. I.R.E.* **41**, 865 (1953).

⁷R. J. Briggs, J. D. Daugherty, and R. H. Levy, *Phys. Fluids* **13**, 421 (1970).

⁸J. H. Malmberg and J. S. deGrassie, *Phys. Rev. Lett.* **35**, 577 (1975).

⁹J. S. deGrassie and J. H. Malmberg, *Phys. Fluids* **23**, 63 (1980).

¹⁰J. H. Malmberg and C. F. Driscoll, *Phys. Rev. Lett.* **44**, 654 (1980).

¹¹R. H. Levy, *Phys. Fluids* **11**, 920 (1968).

Fully Ionized and Total Silicon Abundances in the Alcator-C Tokamak

R. Petrasso, F. H. Seguin, and N. G. Loter

American Science and Engineering, Inc., Cambridge, Massachusetts 02139

and

E. Marmor and J. Rice

Massachusetts Institute of Technology, Cambridge, Massachusetts 02139

(Received 17 September 1982)

With use of x-ray imaging arrays, spatially and temporally resolved measurements were made of fully ionized and total absolute Si ($Z = 14$) densities following injection of Si into Alcator C. The fully stripped ions were detected through x rays resulting from ground-state radiative recombination. Central ion densities were found to be close to coronal equilibrium values. In addition, radial profiles of fully ionized and H-like Si showed large fluctuations during internal disruptions.

PACS numbers: 52.25.Fi, 32.30.Rj, 52.25.Gj, 52.70.-m

Impurity transport in tokamak plasmas is an important process, since it greatly affects plasma properties such as radiative losses.^{1,2} To study this transport, workers have purposely injected nonperturbing, trace amounts of moderate- Z (~ 14) impurities into plasmas.³⁻⁵ Until now such studies have been based on observed radiative emissions from partially stripped impurities, usually integrated along a single chord through the plasma cross section.³⁻⁵ Here we report the first spatially and temporally resolved measurements of fully ionized and total Si ($Z = 14$) abundances, which we made following injection of trace Si into Alcator C. Measurements were also obtained of fluctuations of impurity ion densities due to internal disruptions, a topic addressed only recently.⁶⁻⁸ The method we have used is based in part on detection of continuum x rays, principally from ground-state recombination of the fully stripped ion. (In a different context, fully stripped low- Z impurities, abundant within and intrinsic to the plasma, have been previously measured through charge exchange between fully stripped species and neutral particles.^{9,10}

Very recently this method has been applied, with use of a diagnostic neutral beam, to obtain spatially resolved measurements of C^{+6} and O^{+8} , if one assumes plasma discharge repeatability.¹⁰)

Si was injected, via the laser-blowoff method,³⁻⁵ into Alcator-C plasmas with central temperatures of 1.2 to 1.5 keV. Si transport was monitored by uv and x-ray spectrometers, and by two broadband, absolutely calibrated x-ray diode arrays¹¹ sensitive mainly to plasma radiation from inside a 10-cm radius (limiter radius is 16.5 cm). These arrays, the principal tools of this analysis, were usually filtered differently: The 17-detector "soft"-filtered array ($E \geq 1$ keV), filtered by 10.0 mg/cm² Be, responds mainly $K\alpha$ lines from H- and He-like Si (2.00 and 1.86 keV, respectively); the 10-detector "hard"-filtered array ($E \geq 3$ keV), filtered by 10.0 mg/cm² Be and 32.7 mg/cm² C, responds only to continuum x rays, primarily from ground-state radiative recombination of fully stripped and H-like Si. Even with allowance for the possibility of strong deviations from coronal equilibrium¹² (Fig. 1), fully stripped, H- and He-like ions